THE JOURNAL OF BIOLOGICAL CHEMISTRY VOL. 288, NO. 42, pp. 30559–30570, October 18, 2013

Factor V Activator from *Daboia russelli russelli* Venom Destabilizes β-Amyloid Aggregate, the Hallmark of Alzheimer Disease*

Received for publication, August 17, 2013 Published, JBC Papers in Press, August 28, 2013, DOI 10.1074/jbc.M113.511410

Payel Bhattacharjee[1] **and Debasish Bhattacharyya**[2]

From the Division of Structural Biology and Bioinformatics, Council of Scientific and Industrial Research, Indian Institute of Chemical Biology, Jadavpur, Kolkata 700032, India

Background: β-Amyloid aggregate formation and its destabilization are addressed in Alzheimer disease.
Results: Peptides synthesized using Russell's viper venom factor V activator as a template can destabilize β-amyloid fibril and inhibit cytotoxicity.
Conclusion: These peptides dissociate β-amyloid fibrils to the nontoxic monomeric state.
Significance: This study explores possibility of designed peptides for clinical applications in Alzheimer disease.

Formation of plaque by fibrils of β-amyloid (Aβ) peptide in the brain is the characteristic feature of Alzheimer disease (AD). Inhibition of the process of aggregate formation from Aβ-monomer and destabilization of the aggregate could be useful for prevention and propagation of the disease respectively. Russell's viper venom (RVV) contains protein(s) that destabilize Aβ aggregates as revealed from the thioflavin T assay. The active component was identified as factor V activator (RVV-V). Among the possible mechanisms of destabilization, RVV-V-mediated proteolysis was ruled out from mass spectrometric data and the thioflavin T assay. The alternate hypothesis that small peptides derived from RVV-V destabilize the aggregate is better supported by experimental results. Six small peptides were synthesized using RVV-V as the template, and three unrelated peptides were synthesized to serve as controls. Destabilization of Aβ aggregate by these peptides was studied using spectrofluorometric assays, atomic force microscopy, transmission electron microscopy, and confocal microscopy. Among the peptides, CTNIF and the mixture of the six peptides were most potent in converting the aggregates to the monomeric state and thus, preventing cytotoxicity in SH-SY5Y human neuroblastoma cells. The control peptides failed to show similar effects. Moreover, some of these peptides are stable in blood for 24 h. Therefore, these venom-derived peptides offer an encouraging opportunity to prevent amyloidosis and may provide information to combat AD.

Alzheimer disease (AD)[3] is an age-related degenerative brain disorder leading to cognitive and behavioral dysfunctioning. The aggregation of β-amyloid (Aβ) peptide as extracellular amyloid deposits on the cholesterol-rich regions of neuronal membrane is the primary feature of AD (1, 2). Recent evidences showed that Aβ peptide is generated extracellularly and intracellularly by the enzymatic breakdown of the amyloid precursor protein by β- and γ-secretases. It gives rise to a family of Aβ peptides with variable lengths, among them the 40-residue peptide (Aβ40) is most abundant in normal and AD brains followed by the 42-residue peptide (Aβ42) (3, 4). The intermediate entities *en route* Aβ monomer to the fibrillar state are the soluble oligomers which include small Aβ-derived diffusible ligands and protofibrils. These oligomers are more toxic to cells than mature fibrils (5, 6). The toxicity of the oligomer is attributed to their amphiphilicity, state of aggregation, covalent modifications, and the organization of hydrophobic residues within the oligomeric assembly. Aβ peptide is essential for neuronal cell survival, maintenance of synaptic plasticity, and transfer of day-to-day information through nerve cell networks in the brain (7, 8). In normal human plasma, the metabolism of Aβ peptide is tightly regulated by the soluble form of low density lipoprotein receptor-related protein-1 (sLRP1), which segregates 70–90% of plasma Aβ peptides from brain to plasma. In AD, free Aβ fraction in plasma is increased due to low levels of sLRP1 in plasma. Because in this situation the capacity of sLRP1 to bind Aβ is reduced, there is a decrease in Aβ efflux and increase in Aβ influx across the blood-brain barrier (9). Aβ peptide induces neuronal dysfunction by interaction with cell surface receptors and the receptor for advanced glycosylation end products. Neurotoxic effects of Aβ are elicited by generation of reactive oxygen species, disruption of the cytoskeleton, induction of apoptotic cascades, changing membrane dielectric properties, and ion permeability (10).

Designing of target-specific inhibitors of pathological Aβ aggregates could be useful in the development of therapeutics.

* This work was supported by the Department of Science and Technology, Cognition Science Initiative, Project SR/CSI/07/2009(G) and Council of Scientific and Industrial Research Network Project miND BSC0115.
[1] Supported by a University Grants Commission-National Eligibility Test fellowship.
[2] To whom correspondence should be addressed: Division of Structural Biology and Bioinformatics, Council of Scientific and Industrial Research Indian Institute of Chemical Biology, 4, Raja S.C. Mullick Rd., Jadavpur, Kolkata 700032, India. Tel.: 91-33-2499-5764; Fax: 91-33-2473-0284; E-mail: debasish@iicb.res.in or payel.iicb@gmail.com.
[3] The abbreviations used are: AD, Alzheimer disease; Aβ, β-amyloid; AFM, atomic force microscopy; BBB, blood-brain barrier; DMSO, dimethylsulfoxide; HFIP, 1,1,1,3,3,3-hexafluoro isopropyl alcohol; LDH, lactate dehydrogenase; MS/MS, tandem mass spectrometry; MTT, (3-[4,5-dimethylthiazol-2-yl]-2,5-diphenyltetrazolium bromide); RVV, Russell's viper venom; sLRP1, soluble form of low density lipoprotein receptor-related protein-1; TEM, transmission electron microscopy.

Recent reports showed that low molecular weight drugs including small organic molecules, peptides, small molecular chaperones, enzymes, and antibodies are gaining attention for the treatment of AD (11–13). The concept of using proteases and peptides as therapeutic agents is common. High potency and selectivity of peptides for molecular targets make them very attractive in the process of drug designing (14, 15). A majority of the new drugs have evolved from the secondary metabolites of natural products or from compounds derived from natural products (16). Snake venoms are enriched with peptides, proteins, and other molecules with highly specific biological function. Elucidation of the structure and function of these molecules would lead to the development of new therapeutic molecules. Angiotensin-converting enzyme inhibitors, exenatide, and chlorotoxin are examples of knowledge-based approach of drug designing from proteins/peptides of various venoms (17).

Daboia russelli russelli is a subspecies of Russell's viper which is found in the Eastern India at the West coast of the Bay of Bengal. Russell's viper venom is a rich source of phospholipase A_2 isoforms, coagulation factor V- and X-activating proteases, hyaluronidases, nuclease, protease inhibitors, hemorrhagic toxins, and several other constituents (18). In recent years, venom research is not confined to neutralization of venom toxicity to save lives of victims but also includes search for pharmacologically active compounds. Some venom components are available commercially as a constituent of diagnostic test kit or as therapeutic agent (19, 20). During our investigation on the proteolytic activity of the venom from *D. russelli russelli*, we observed that the venom contains protein(s) that specifically cleave the aggregates rather than the monomeric forms of BSA and Aβ40 peptide. The causative molecule was purified and identified as the coagulation factor V activator (RVV-V). Elucidation of the mechanism of destabilization of Aβ aggregate by RVV-V is important to address the potency of this molecule as an antiaggregant. The initial observations showed that RVV-V did not disintegrate the fibril through proteolysis; rather, few specific sequences of RVV-V might interact with the Aβ oligomer/aggregate restoring the monomeric state and inhibiting further elongation of the fiber. Because the sequence QKLVFFA, residues 15–21, is the central hydrophobic region of Aβ peptide and prone to form a β-sheet structure, the self-interacting property of Aβ peptide has been exploited to design a few small peptides using RVV-V as a template which shows sequence homology with this region of Aβ peptide. The small synthetic peptides were tested *in vitro* for their ability to inhibit the formation of Aβ fibrils. Finally, the effect of the peptides inhibiting Aβ-induced toxicity to the human neuroblastoma SH-SY5Y cells was investigated.

EXPERIMENTAL PROCEDURES

Materials—Fine chemicals were procured as follows: CM-Sephadex C-50, DMSO, glycine, HFIP, phenyl-Sepharose 4B, thioflavin T, TFA, Triton X-100, trypan blue, and dialysis tubing cellulose membrane (25-mm diameter; cut-off range 12 kDa) were from Sigma. A prestained protein molecular mass ladder for SDS-PAGE (PageRuler, 10–170 kDa) was from Fermentas. Dulbecco's modified Eagle's medium (DMEM), Ham's modification of F-12, PBS (pH 7.2), heat-inactivated FBS, MTT, L-glutamine, penicillin/streptomycin, gentamycin, Fungizone, and trypsin solution were from Invitrogen. Mica sheets used in AFM (ASTM grade ruby mica, size 20 × 20 mm, 0.27–0.33-mm thickness) were from Mica Fab, Chennai, India. Carbon-coated copper grids (GSCu300C) used in TEM were from ProSciTech, Australia. Aβ40 and Aβ42 (>95% purity demonstrated by mass spectrometry and RP-HPLC) were from American Peptide Company. Antibodies and the LDH assay kit were from Abcam. Alexa Fluor 633-labeled goat anti-rabbit IgG secondary antibody was from Molecular Probes. HPLC grade solvents, Tris, and glacial acetic acid were from SRL, Mumbai, India. RVV was procured from Dipak Mitra, a licensed trophy of Calcutta Snake Park, as desiccated yellowish shinning crystals that contain ~60% protein (w/w).

Purification of RVV Component—Dry venom (20 mg, equivalent to 12 mg of protein) was suspended in 1 ml of 20 mM sodium phosphate, pH 7.5, for 30 min at 4 °C. Tissue debris was removed by centrifugation at 8085 × *g* using a 5810 R bench top centrifuge (Eppendorf) at 4 °C. The clear yellowish supernatant was applied to CM-Sephadex C-50 column (60 mm × 20 mm) preequilibrated with the same buffer at 25 °C. Unabsorbed fractions were eluted after washing with 3 column volumes of the equilibrating buffer. Bound fractions were eluted after application of a linear gradient of 0–1.0 M NaCl in the same buffer in 3 column volumes. After completion of the gradient, elution was continued with the buffer containing 1.0 M NaCl when an additional sharp peak appeared.

The last fraction of the previous chromatography was pooled and dialyzed overnight at 4 °C against 20 mM sodium phosphate, pH 7.5, containing 1.0 M ammonium sulfate. The dialyzed sample applied to a phenyl-Sepharose CL-4B column (40 mm × 7.5 mm) preequilibrated with the same buffer at 25 °C. Unabsorbed fractions were eluted after washing with 3 column volumes of equilibrating buffer. Bound fractions were eluted after application of reverse gradient of 1.0–0 M ammonium sulfate in the same buffer. In either of the chromatographies, the flow rate was 20 ml/h, fraction size was 1 ml, and elution was followed at 280 nm. The activity of the chromatographic fractions was followed by running PAGE of BSA aggregates preincubated with the fractions and observing the digestion pattern of the aggregate after staining and destaining.

Electrophoresis—12% PAGE and 10% SDS-PAGE were performed for protein profiling using standard laboratory protocols. Staining was done using 0.25% (w/v) Coomassie Blue R-250 stain followed by destaining with water/methanol/acetic acid (5:4:1, v/v).

MALDI-TOF Analysis—Mass analysis was performed using 4800 MALDI TOF/TOF (model 4800, Applied Biosystems) instrument operated in reflectron mode. For MS/MS analysis proteins were digested by trypsin (gold) (21). Protein samples were desalted using C_{18} zip-tip cartridge (Millipore), and mass analysis was done using a saturated solution of α-cyano-4-hydroxycinnamic acid in 50% acetonitrile/0.1% TFA. The MS/MS peaks of the most intense mass ions were searched against SwissProt and NCBInr Database using Mascot software (Matrix Science Ltd., London, UK).

Amino Acid Sequencing—Electroblotting of protein sample to PVDF membrane was performed after electrophoresis of the

purified component (5 μg) in 15% SDS-PAGE. The gel was rinsed in transfer buffer (10 mM CAPS, pH 11.0, containing 10% methanol) for 5 min. Simultaneously, PVDF membrane with the same size as that of gel was allowed to soak in 100% methanol for 10 s then was rinsed with water for 5 min followed by equilibration of the membrane in transfer buffer for 30 min. Gel and membrane were sandwiched between fiber pad and filter papers, and the assembled transfer cassette was submerged into the tank with the gel on the cathode side and the membrane on the anode side. The purified component was transferred to the membrane electrophoretically at a constant voltage of 90 for 2.5 h. After transfer, the membrane was rinsed several times with water to remove the buffer and was treated with 100% methanol for 2–3 s. Blotted component was visualized with 0.2% Ponceau S in 1% acetic acid.

N-terminal sequencing of blotted component was carried out using a Procise 491 protein-peptide sequencing system with on-line PTH (phenylthiohydantoin) analyzer (model 491C; Applied Biosystems). The amino acid present at a particular residue number was determined by comparing retention time of PTH derivatives of cleaved amino acid from the N terminus of the test protein sample with the retention times of the standards. This process was repeated sequentially to provide the N-terminal sequence of the protein.

Synthetic Peptides—The peptides, DVPH (designated as R_1; 466.50 Da), VPH (R_2; 351.41 Da), HCTNIF (R_3; 733.85 Da), CTNIF (R_4; 596.71 Da), TNIF (R_5; 493.57 Da), and NIF (R_6; 392.48 Da) were designed using the sequence of RVV-V as a template, and a few nonspecific peptides like SVLQ (NS_1; 445.5 Da), LPI (NS_2; 341.46 Da), and VLQ (NS_3; 358.45) were designed using the sequence of functionally similar protein of RVV-V as a template. The peptides were synthesized by a solid phase technique and purified by reverse-phase HPLC (GenPro Biotech, New Delhi, India). Purity of the peptides (>98%) was ascertained from amino acid sequencing and laser desorption mass spectrometry as provided by the company.

Soluble Aggregates of Proteins—BSA (10 mg/ml in 20 mM sodium phosphate, pH 7.5) was heated at 80 °C for 30 min when soluble aggregates were formed without precipitation. Aβ40/42 peptide (3.0 mg/ml) was dissolved in HFIP, sonicated in a water bath for 10 min, put into aliquots in polypropylene microcentrifuge tubes, and kept at 25 °C until it became a clear solution. The solution was then dried under vacuum and stored at −20 °C. Prior to use, the thin film of HFIP-treated Aβ40/42 peptides were dissolved in DMSO and diluted to 100 μM by 10 mM sodium phosphate, pH 7.5, containing 100 mM NaCl. It was incubated at 37 °C with mild shaking to form soluble aggregates. For treatment of SH-SY5Y cells, HFIP and DMSO treatments were followed as mentioned and diluted to 100 μM by PBS containing 0.1% SDS to form Aβ40/42 soluble oligomers. Under this condition, formation of elongated fibril is restricted.

Fibrillogenesis Assay—Fibrillar structure of Aβ40/42 aggregate was followed using thioflavin T that forms highly fluorescent complexes with amyloid and amyloid-like fibrils after interacting with the β-sheet regions of the proteins (ex: 450 nm; em: 480–600 nm) (22, 23). Aliquots of Aβ40/42 aggregate (10 μM) with or without proteins/peptides were added to thioflavin T (0.1 μM) where the volume was made up to 1 ml by 10 mM sodium phosphate, pH 7.5. The emission maximum was invariable at 485 nm, and the bandwidth was 10/10 nm. A Hitachi F-7000 spectrofluorometer was used. Each reading represented the average of three values after subtracting the contribution from inhibitors.

Stability of Peptides in Vitro—The assay was performed according to Adessi *et al.* (24) with modifications. The rat blood plasma solution was prepared in PBS containing 0.5% Triton X-100. The peptides (1 mM in PBS) were diluted to 100 μM in freshly prepared plasma solution. The solution was incubated at 37 °C for 24 h. Proteolysis, if any, was arrested by 1 μM protease inhibitor mixture (Calbiochem). The plasma proteins, but none of the peptides, were precipitated by the addition of 100 μl of cold methanol (sample: MeOH = 1:4, v/v) and kept at 4 °C for 1 h. The precipitate was centrifuged at 10,000 × *g* for 10 min at −20 °C, and the supernatant containing the peptide was analyzed by a RP-HPLC Nova Pak C_{18} (3.9 mm ×150 mm, 4 μm) symmetry column. The column was equilibrated with water containing 0.1% TFA, and a linear gradient up to 70% acetonitrile containing 0.1% TFA in 40 min was applied. Flow rate was 0.7 ml/min, and 50 μl of sample was injected. Elution of peptides was monitored at 220 nm. Relative areas under the peaks were considered as its respective abundance. A blank run without sample ensured absence of artifacts in the chromatogram.

Cell Culture—Human SH-SY5Y neuroblastoma cells were maintained in medium containing DMEM/Ham's modification of F-12 (1:1 v/v) supplemented with 10% FBS, 2 mM L-glutamine, 1% penicillin/streptomycin, gentamycin antibiotics, and 0.2% Fungizone as an antimycotic agent. The cells were routinely subcultured and grown at 37 °C in a humidified incubator with 95% air/5% CO_2 in tissue culture flasks.

AFM—Protein samples were adsorbed on a highly ordered pyrolytic graphite surface, and acoustic alternative current mode AFM was performed. A Pico plus 5500 AFM instrument (Agilent Technologies) attached with a piezoscanner of maximum range of 9 μm and 225-μm long microfabricated silicon cantilevers (Nanosensors) were used. The nominal spring force constant was 21–98 Newtons/m. The cantilever resonance frequency of 150–300 kHz was tuned into resonance frequency. Cells were seeded on to glass coverslips having density of 10^6 cells/well in a 6-well plate. The cells were treated with medium containing 5 μM Aβ40/42 preincubated for 24 h with or without 5 μM synthetic peptides. The same volume of medium was added to control cultures. The cells were incubated for an additional period of 48 h at 37 °C. Cells attached on the coverslip surface were imaged in liquid mode using a 100-μm scanner. Cantilevers of 450 μm length with a nominal spring force constant of 0.2 Newton/m were used. The resonance frequency was set at 13 kHz. The individual plots shown for the surface topography of the various samples are representative views of the morphologies observed for multiple areas of the samples. The images (512 × 512 pixels) were executed using Pico scan software (Molecular Imaging).

TEM—The monomeric and aggregated states of protein samples were distinguished by TEM. In brief, 10 μl of the sample (100 μM) was placed on a carbon-coated 300-mesh grid for 1 min at ambient temperature, and the unbound substrate was removed by a blotting paper. To stain the adhered particles,

the grid was treated with 2% uranyl acetate for 20 s, and the excess reagent was removed by a blotting paper. The grid was dried for 15 min, and the sample was viewed under TEM (model FEI TECNAI G2 Spirit BioTwin, Czech Republic) at an opening voltage of 60 kV with ×40,000 magnification.

Confocal Microscopy—The cells were washed twice with PBS, fixed for 20 min using 4% formaldehyde at 25 °C, and permeabilized in 0.1% Triton X-100 for 10 min, and the nonspecific protein binding sites were blocked by 1% BSA for 1 h. The protein of interest was detected using the rabbit polyclonal Aβ(1–42) or Aβ(1–40) antibody (1:200 dilution) followed by Alexa Fluor 633-labeled goat anti-rabbit IgG (1:500 dilution), and the nucleus was counterstained with 0.01% DAPI. Confocal images were collected using an Andor spinning disc confocal microscope (Yokogawa CSU-X1) equipped with Andor ixon3 897 EMCCD camera and Olympus ix81 microscope.

MTT Assay—Cells were harvested from flasks and plated in 96-well polystyrene plates (Corning Inc., Corning, NY) with ~10^5 cells/100 μl of medium per well. The plates were incubated at 37 °C for 24 h to allow the cells to attach. Aβ40/42 (10 μM) preincubated with or without synthetic peptides for 24 h was diluted with fresh medium and added to individual wells. The same volume of medium and medium containing 0.01% SDS was added to cultures to serve as controls. The plates were then incubated for an additional period of 48 h at 37 °C. Cell viability was determined with addition of 10 μl of 5 mg/ml MTT to each well (25). After incubation for 4 h at 37 °C, the medium was aspirated from each well, and 100 μl of DMSO was added to each well. Plates were agitated at 25 °C for 10 min to dissolve crystals. The absorbance at 595 nm was measured by a multiwell assay plate reader (BioTek-Epoch; BioTek Instruments). Averages absorbance values of three replicate wells were used for each set, and each experiment was repeated three times. In this assay, the cells without any test samples but with MTT served as positive control, and the cell where no MTT was added served as negative control. The difference of absorbance was considered as 100% viability of cells.

LDH Assay—The release of LDH due to cell membrane damage (cytotoxicity) was quantified by LDH assay kit following the manufacturer's protocol (Abcam). Briefly, 10^5 cells/100 μl were plated in 96-well polystyrene plates and incubated at 37 °C for 24 h. Samples as described in the previous section were added to the wells and incubated for an additional period of 48 h at 37 °C. The plate was then centrifuged at 10,000 × *g* for 15 min at 4 °C. One nonsterile 96-well plate was set aside and labeled as an assay plate for each experimental set. Supernatants (50 μl) were transferred from the top of the wells of the culture plate to the assay plate. A mixed detection kit reagent (50 μl) was then added to each of the assay wells on top of the supernatant in rapid succession. The total volume in each well was 100 μl. NADH (0, 2.5, 5.0, 7.5, 10.0, and 12.5 nmol) served as standard. The absorbance was taken after 30 min at 450 nm using a multiwell assay plate reader. The initial reading of each set was subtracted from the final reading to calculate formation of NADH using the calibration curve. LDH activity of the samples was calculated as follows: LDH activity (milliunits/ml) = amount of NADH in nmol × sample dilution/time interval × sample volume.

Trypan Blue Cell Viability Assay—Cell viability was investigated by trypan blue dye exclusion test (26). 10^6 cells/ml were plated in 24-well plates. After 24 h, test samples were added and incubated for an additional 48 h at 37 °C. The cells were trypsinized, centrifuged for 5 min at 1000 × *g* and resuspended in PBS. Trypan blue solution (0.4%) was added to the cells (1:1, v/v), mixed thoroughly, and allowed to stand for 5 min. Cells were counted in dual chambers by a hemocytometer under light microscope. The cell viability percentage was calculated using the formula: percentage of cell viability = (viable cell count/total cell count) × 100.

Statistical Analysis—All data in this study are expressed as mean ± S.D. Significant differences of data were calculated by Student's *t* test after analysis of variance. Probability values of $p < 0.05$ were considered to represent significant differences.

RESULTS

Purification and Identification of Aggregate Destabilization Factor from RVV—In search for a proteolytic enzyme from RVV, PAGE analysis was performed using BSA solution (5 μg) preincubated with RVV (2–10 μg of total protein). It was found that the enzyme destabilized the high molecular mass aggregates of BSA rather than its monomeric form. For confirmation, soluble BSA aggregate was prepared under controlled experimental conditions. The monomer and aggregate were incubated with RVV separately for 24 h at 37 °C, and PAGE was performed. The electrogram clearly showed that the enzyme has greater tendency toward destabilization of the aggregates than the monomer (Fig. 1*A*). PAGE was performed after each step of chromatography of RVV to identify the aggregate destabilizing component. In the first step, the venom solution was applied to a CM-Sephadex C-50 column at pH 7.5 where two fractions F1 and F2 were partially resolved as unbound components, and two more fractions F3 and F4 were well resolved as bound components after application of 0–1.0 M NaCl gradient (Fig. 1*B*). Disaggregation property was confined to F4. The SDS-PAGE revealed that F4 fraction contained three components (*inset*, Fig. 1*B*). F4 was further fractionated by hydrophobic interaction chromatography using a reverse gradient of 1.0–0 M ammonium sulfate. In this step, four fractions (denoted as P1–P4) were well resolved where the activity was retained by P4 (Fig. 1*C*). The activity of the RVV fractions was also demonstrated by incubating 10 μl of Aβ40 (10 μM) aggregate with 1 μl of the four fractions of RVV (P1–P4, protein concentrations in each being 5 ± 0.5 μg/ml) for 24 h at 37 °C. The extent of amyloid fibril formation was quantified using thioflavin T assay. P4 showed highest inhibition of aggregation (Fig. 1*D*). The results are presented as the percentage inhibition of aggregate formation considering the fluorescence intensity of Aβ40 as 100%. The purity and molecular mass of P4 were checked by SDS-PAGE where it appeared as a single band of 28 kDa (*inset*, Fig. 1*C*). The MALDI-TOF analysis showed the appearance of two closely spaced peaks of 28,363.53 and 28,361.13 Da, which indicates the presence of two polypeptide chains or subunits of a protein (Fig. 1*E*).

The amino acid sequences of the purified component of RVV derived from MS/MS analysis, *viz.* EWVLTAAHCDR, WCEPLYPWVPADSR, and ISTTEDTYPDVPHCTNIFIVK, showed

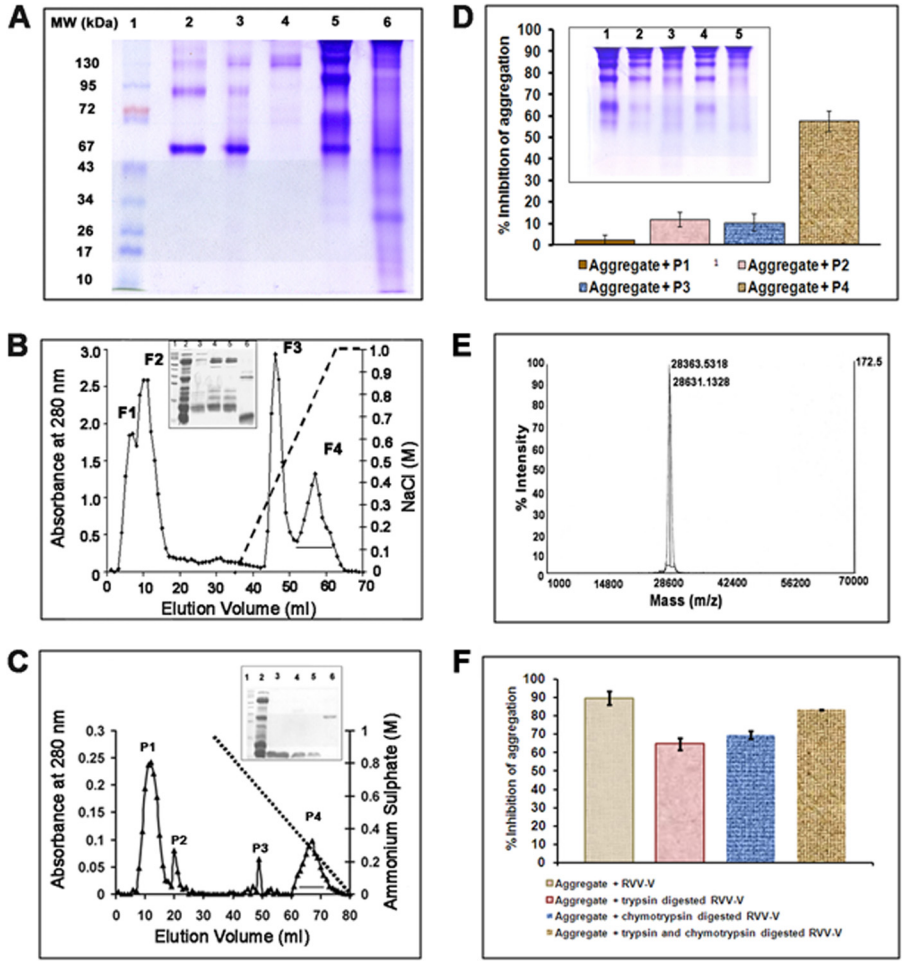

FIGURE 1. **Destabilization of protein aggregates by RVV and purification of the component.** *A*, 10% PAGE. *Lane 1*, prestained markers. The molecular masses are indicated. *Lane 2*, commercially available BSA (5 μg). *Lane 3*, BSA (5 μg) incubated with RVV (5 μg) for 24 h at 37 °C. *Lane 4*, RVV (5 μg). *Lane 5*, BSA aggregate (25 μg). *Lane 6*, BSA aggregate (25 μg) incubated with RVV (5 μg) as stated earlier. *B*, purification of the aggregate destabilizing component of RVV by CM-Sephadex C-50 where a linear gradient of 0–1.0 M NaCl was applied (*dotted line*). The *bar* represents the active fraction (F4). *Inset*, 15% SDS-PAGE. *Lane 1*, prestained molecular mass markers. *Lane 2*, RVV. *Lanes 3-6*, fractions F1–F4. *C*, hydrophobic interaction chromatography of F4, where the *dotted line* represents the reverse gradient of 1–0 M ammonium sulfate, and the *bar* represents the active fraction. *Inset*, 15% SDS-PAGE. *Lane 1*, prestained molecular mass markers. *Lane 2*, RVV. *Lanes 3*-6, fractions P1–P4. *D*, destabilization of preformed Aβ40 aggregate (10 μM) by the fractions P1–P4. *Inset*, BSA aggregate (25 μg) destabilized by the fractions. *E*, electrospray ionization-MS of RVV P4 indicating presence of two closely spaced peaks. *F*, destabilization of Aβ40 aggregate (10 μM) with P4 (1 μM) and proteolytically digested P4 (1 μM). P4 was identified as RVV-V. The *error bars* represent mean ± S.D. of three independent experiments.

TABLE 1
Assignment of the purified protein isolated from Russell's viper venom to protein families by MS/MS

Protein name	Accession no.	Protein score C.I.%	Peptide ion m/z^a	Sequence	MS/MS-derived sequence
(P18965) *Vipera russelli* proteinase RVV-V (EC 3.4.21.95) (factor V-activating proteinase α)	VSPG_DABRU	100	1357.5095	36–46	EWVLTAAHCDR
			1775.6656	151–164	WCEPLYPWVPADSR
			2449.9934	128–148	ISTTEDTYPDVPHCTNIFIVK

[a] Because the charge (z) is 1, m/z values correspond to the mass of the peptides.

high sequence homology with the stretch of sequences of 36–46, 151–164, and 128–148 residues of the α-subunit of factor V activator from *Vipera russelli* (protein score 100, Table 1). The N-terminal sequence analysis by Edman degradation up to 15th residue of P4 revealed VVGGDECNINEHPFL. It exactly matched with the sequence of factor V activator (RVV-V) of venom reported previously from other subspecies of Russell's viper (27). The molecule is, therefore, denoted as RVV-V.

Designing of Synthetic Peptides Using RVV-V as Template—It is assumed that there are two probable mechanisms by which the preformed Aβ aggregate may be destabilized. RVV-V specifically activates factor V of blood coagulation cascade of envenomated animals by cleaving a single peptide bond between Arg^{1545} and Ser^{1546} (27). RVV-V being a proteolytic enzyme, it may cleave at specific sites of the Aβ40/42 peptide residing in the preformed aggregate leading to its disintegration. The Aβ40/42 peptide lacks this specific sequence. Therefore, proteolysis of the preformed fibril by RVV-V is a remote possibility. Alternatively, a specific stretch of the amino acid sequence of RVV-V might have strong affinity for a certain stretch of the Aβ40/42 peptide particularly of the region QKLVFFA (residues 15–21) that is considered as the sticky zone responsible for adhesion, *i.e.* aggregation. Further, more

```
CLUSTAL 2.0.12 multiple sequence alignment


RVV-V       VVGGDECNINEHPFLVALYTSASSTIHCAGALINREWVLTAAHCDRRNIRIKLGMHSKNI
Aβ1-42      ------------------------------------------------------------


RVV-V       RNEDEQIRVPRGKYFCLNTKFPNGLDKDIMLIRLRRPVTYSTHIAPVSLPSRSRGVGSRC
Aβ1-42      ------------------------------------------------------DAEF
                                                                     .:.
                                  141     147
RVV-V       RIMGWGKISTTEDTYPDVPHCTNIFIVKHKWCEPLYPWVPADSRTLCAGILKGGRDTCHG
Aβ1-42      R---------HDSGY-EVHHQKLVFFAED----------------------------VG
            *          :. * :* * . :*:.:.                             *
                                  15     21
RVV-V       DSGGPLICNGEMHGIVAGGSEPCGQHLKPAVYTKVFDYNNWIQSIIAGNRTVTCPP 236
Aβ1-42      SNKGAII------GLMVGG-----------------------VVIA--------- 42
            .. *.:*      *::.**                        :**
```

FIGURE 2. **Multiple alignments of sequences of α-polypeptide of RVV-V with Aβ42 peptide.** The FASTA format sequence of the two polypeptides was aligned using ClustalW, in which Gonnet was used as default alignment matrix. The default parameter for gap open and gap extension penalty were 10 and 0.1, respectively.

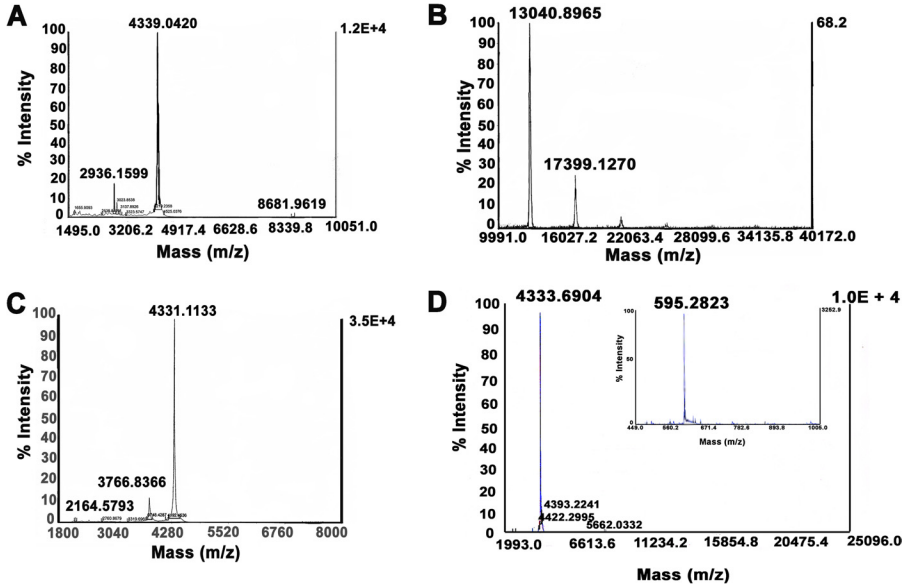

FIGURE 3. **MALDI-TOF analysis.** *A*, Aβ40 monomer. *B*, Aβ40 oligomer. *C*, Aβ40 oligomer treated with RVV-V. *D*, Aβ40 oligomer treated with R_4 peptide. *Inset*, R_4 peptide.

than one specific stretch of RVV-V may intercalate into the β-pleated sheet of the aggregate causing its destabilization. To elucidate this, the following experiment was performed. 100 μl of RVV-V (50 μM) was digested separately with trypsin, chymotrypsin, and a mixture of both for 24 h at 37 °C. RP-HPLC and MALDI-TOF analysis showed generation of smaller peptide fragments of RVV-V ranging from 900 to 2000 Da and absence of 28 kDa of undigested RVV-V (data not shown). Fibrillogenesis assay using thioflavin T was performed by incubating 10 μl of preformed Aβ40 aggregate (10 μM) with 5 μl of RVV-V (1 μM) and 5 μl of the digested RVV-V (1 μM) in 1 ml for 24 h at 37 °C where RVV-V as well as RVV-V-derived peptides showed destabilization of aggregation. This result indicated that not only the intact RVV-V but also small peptides so generated from it were also capable of destabilizing the aggregate (Fig. 1*F*).

The ClustalW multiple sequence alignment of RVV-V (α-polypeptide) with Aβ42 peptide revealed significant sequence homology, especially between the 15–21 residues of Aβ42 peptide and 141–147 residues of RVV-V (Fig. 2). The potential cleavage site on RVV-V by trypsin and chymotrypsin was predicted using Expasy peptide cutter tool, which showed generation of peptides of variable lengths. Among them, a peptide corresponding to 141–147 residues of RVV-V was also present. Using these selected regions of RVV-V as a template, six small peptides of 300–800 Da, *viz.* R_1, R_2, R_3, R_4, R_5, and R_6, were synthesized. Corresponding sequences were described under "Experimental Procedures." Few additional peptides, *viz.* NS_1, NS_2, and NS_3 were also synthesized to serve as nonspecific controls.

Disaggregation followed by MS Analysis—Interactions of soluble oligomeric Aβ40 with RVV-V and all other peptides were followed by MS analysis. The soluble small oligomers are not only intermediate entities toward aggregate formation, they are strongly cytotoxic too; *e.g.* the trimer and the tetramer are ~8- and 13-fold more toxic than the monomer Aβ peptide (28). Physical homogeneity of the monomeric Aβ40 has been demonstrated in Fig. 3*A* where it appeared as a single mass of 4339

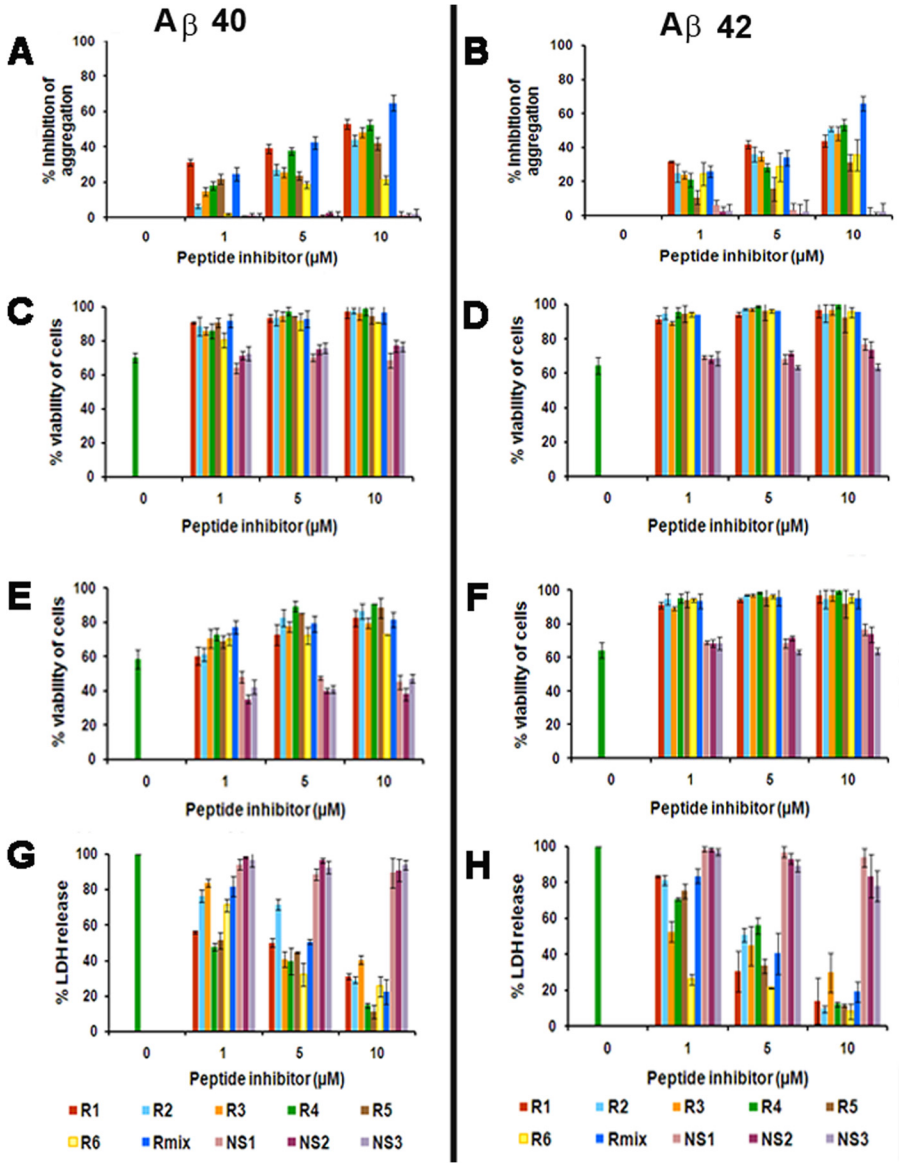

FIGURE 4. **Disassembly of preformed Aβ40/42 aggregate and inhibition of cytotoxicity.** *A* and *B*, thioflavin T assay. Aβ40 and Aβ42 fibrils (10 μM) were disassembled by peptides (1–10 μM) after 24 h of incubation at 37 °C. The intensity of Aβ40/42 aggregate in absence of any peptide was considered as 100%, whereas for buffer it was 0%. *C–H*, prevention of Aβ40 and Aβ42 (10 μM)-induced toxicity by peptides (1–10 μM) on neuroblastoma cells. *C* and *D*, cell viability count using trypan blue dye exclusion test. *E* and *F*, MTT assay. In viability assays, the cell count or absorbance of the untreated cells was considered as 100%. *G* and *H*, LDH assay. The LDH released from the Aβ40/42 oligomer-treated cells was considered as 100%, whereas a blank devoid of Aβ40/42 and peptides served as 0%. The values of the medium containing 0.01% SDS-treated cells were subtracted from the test samples. In all presentations, the *color bars* represent inclusion of peptides as described in the *bottom*. The *bars* represent mean ± S.D. of three independent experiments.

Da. The oligomers generated from the monomer showed the presence of the trimer along with decreasing amounts of the tetramer, pentamer, and hexamer (Fig. 3*B*). However, when these oligomers were treated separately with RVV-V and the synthetic peptides and the products formed were analyzed, only the monomer and no higher mers could be detected (Fig. 3, *C* and *D*). Further, the RVV-treated sample did not show generation of degraded products of Aβ40 arising from proteolysis. In the same analysis, the existence of the free peptide corresponding to 595 Da was also detected (a representative profile with R4 has been shown in Fig. 3*D*, *inset*). These collectively indicate that the peptides interact with the oligomers, the [oligomer-peptide] adducts are unstable, and it is dissociated to such an extent that the adduct remains undetectable at least in MS analysis.

Destabilization of Aggregates in Vitro—Destabilization of preformed Aβ40/42 amyloid aggregate (10 μM) was followed by incubation with 1–25 μM synthetic peptides or a mixture thereof for 24 h at 37 °C. Thioflavin T assay showed disassembly of preformed aggregates by synthetic peptides in a dose-dependent manner both for Aβ40/42 (Fig. 4, *A* and *B*). Among these peptides, 10 μM R_1, R_2, R_4, and R_{mix} showed 44.7 ± 3.8, 51.0 ± 1.6, 53.4 ± 3.5, and 65.8 ± 4.2% of destabilization of Aβ42 aggregation, respectively (Fig. 4*B*). A further increase of concentration of inhibitory peptides or incubation time did not show significant enhancement of disaggregation. The nonspecific peptides (NS_1–NS_3) serving as control had little or no effect on the destabilization of the aggregate.

Prevention of Aβ-induced Cytotoxicity—Inhibition of Aβ oligomer-induced cytotoxicity by the peptides was quantified by

TABLE 2
Stability of synthetic peptides *in vitro*

Inhibitor peptides	100% stability in rat plasma
	h
R_1	0.5
R_2	0.5
R_3	20
R_4	24
R_5	24
R_6	0.5
R_{mix}	20

incubating preformed Aβ40/42 oligomer (10 μM) with 1–25 μM synthetic peptides for 24 h at 37 °C. Thereafter, SH-SY5Y cells were treated with the Aβ40/42 aggregate itself or pretreated with synthetic peptides. Finally, cell viability was estimated using the trypan blue dye exclusion test and MTT assay. All of the venom-derived peptides showed 10–20% increase in cell viability compared with the Aβ oligomer-treated cells in the trypan blue viability test (Fig. 4, *C* and *D*); but this test is not adequate to demonstrate the protective effect of peptides on cells because the assay cannot distinguish between healthy and morbid cells. Alternately, the MTT assay was employed which showed good inhibition of oligomer-induced cytotoxicity by the synthetic peptides (Fig. 4, *E* and *F*). Among them, R_4 and R_5 at 10 μM increased the cell viability to 90.98 ± 3.33 and 88.49 ± 4.70%, respectively, compared with Aβ42-treated cells (Fig. 4*F*). Reduction of cell viability by the peptides at 25 μM was 5–15% compared with untreated cells. This illustrates the nontoxic character of the peptides (data not shown).

The LDH assay showed significant inhibition of Aβ40/42 oligomer-induced LDH release by the synthetic peptides (Fig. 4, *G* and *H*). While considering LDH released by the Aβ42 oligomer-treated cells as 100%, the release by the peptides R_2, R_4, and R_6 at 10 μM was 9.7 ± 1.8, 12.3 ± 1.4, and 8.3 ± 5.5% respectively (Fig. 4*H*). The nonspecific peptides failed to prevent Aβ-induced cytotoxicity in the cultured cells.

Stability of Synthetic Peptides—The peptides were incubated *in vitro* with rat plasma to evaluate their stability in mammalian circulatory system. Although small peptides are usually devoid of proteolytically hydrolyzable sequences, they are prone to self- or co-aggregation. The average retention times of R_1, R_2, R_3, R_4, R_5, and R_6 are 5.00 ± 0.01, 3.46 ± 0.02, 22.83 ± 0.01, 24.13 ± 0.10, 22.32 ± 0.12, and 22.27 ± 0.04 min, respectively, in the RP-HPLC system employed here. The results indicated that the most stable peptides are R_3, R_4, R_5, and R_{mix}. These peptides showed very little or no degradation during the test period of 24 h, and their R_t correspond to untreated peptides (Table 2).

Microscopic Analysis of Aggregation and Its Destabilization—Direct visualization of protein and cells under various microscopes leads to better understanding of the cellular and biochemical processes. R_{mix} showed maximum inhibition of Aβ40/42 fibrillogenesis and cytotoxicity. Therefore, the effect of RVV-V, R_{mix}, and a nonspecific peptide (NS_1) on the assembly process of Aβ40/42 was investigated by TEM and AFM. Fig. 5*A* shows TEM images of Aβ42 monomer, in which Aβ42 was diluted from DMSO stock solution into buffer at 5 μM and put onto the carbon-coated grid immediately before imaging. Only small globular structures were observed. In contrast, large fibrillar aggregates were detected after incubation of prefibrillized Aβ40/42 for 7 days at 4 °C (Fig. 5, *B* and *C*). When this prefibrillized Aβ42 was incubated with R_{mix} (1 μM), it showed a distinct morphological difference from the aggregates. In this case, whereas mature fibril formation was decreased, the occurrence of monomers and structures of intermediate multimeric entities was detected in the presence of the inhibitors (Fig. 5, *D* and *E*). However, the fibrillar morphology of Aβ42 was retained after incubation with NS_1 (Fig. 5*F*). The same samples were analyzed in AFM, and results supported the morphological analysis obtained from TEM. The AFM analysis showed the appearance of the Aβ40/42 monomer as small spherical particles of 35–45-nm diameter (Fig. 5*G*), whereas the corresponding fibrils appeared as a "beads on a string"-like morphology having an approximate width of 150 nm (Fig. 5, *H* and *I*). This distinct fibril of Aβ42 was disrupted by RVV-V and R_{mix} to form smaller oligomer and monomers of 40–65-nm diameter as shown in Fig. 5, *J* and *K*. As expected, NS_1 was unable to disintegrate the fibrillar morphology of Aβ42 (Fig. 5*L*).

The topographs of SH-SY5Y cells in AFM revealed the appearance of clumps of aggregates on cellular surface upon incubation of cells with preformed Aβ40/42 aggregate (10 μM) for 48 h compared with the clear surface of untreated cells (Fig. 6, *A–C*). In contrast, when the Aβ42 aggregate (10 μM) was incubated with R_{mix} (1 μM) for 24 h at 37 °C, applied to cells, and incubated for additional 48 h, the micrograph did not show presence of aggregate on cell surface (Fig. 6*D*). The peptide NS_1 as control was unable to dissociate the aggregates from the cell surface (Fig. 6*E*). The soluble oligomers of Aβ40/42 are localized within the perinuclear cytosol and extracellular space (4). Therefore, prevention of cellular localization of soluble oligomer may reduce cytotoxicity. Immunocytochemical analysis was performed by incubating the Aβ40/42 soluble oligomer (10 μM) with or without peptide for 24 h at 37 °C. Then the SH-SY5Y cells were treated with the samples for an additional period of 48 h at 37 °C. The confocal images of Aβ42-treated cells were different from untreated cells and cells treated with Aβ42 preincubated with synthetic peptides. The Aβ40/42 oligomer-treated cells showed high expression of Aβ40/42 oligomer localized within the cytosol and the nucleus, whereas untreated cells showed faint expression of intrinsic Aβ42 peptide (Fig. 6, *F–H*). The morphology of cells were somewhat distorted compared with control cells of typical elongated morphology. When the Aβ42 oligomer was preincubated with R_{mix} and applied to cells, the cells showed very faint expression of Aβ42, indicating that the mixture of synthetic peptides might be blocking the β-sheet region of Aβ42, preventing its further extension, or they might be preventing the oligomer from entering the cells through membrane-bound receptors (Fig. 6*I*). Whatever may be reason, the R_{mix} successfully inhibited the Aβ-induced cytotoxicity. However, NS_1–NS_3 was ineffective in the prevention of localization of toxic oligomer into the cell (Fig. 6*J*). Therefore, destabilization of preformed fibrils by the synthetic peptides was specific.

DISCUSSION

This study demonstrates the ability of RVV-V-derived small peptides toward disruption of preformed Aβ-amyloid fibrils as

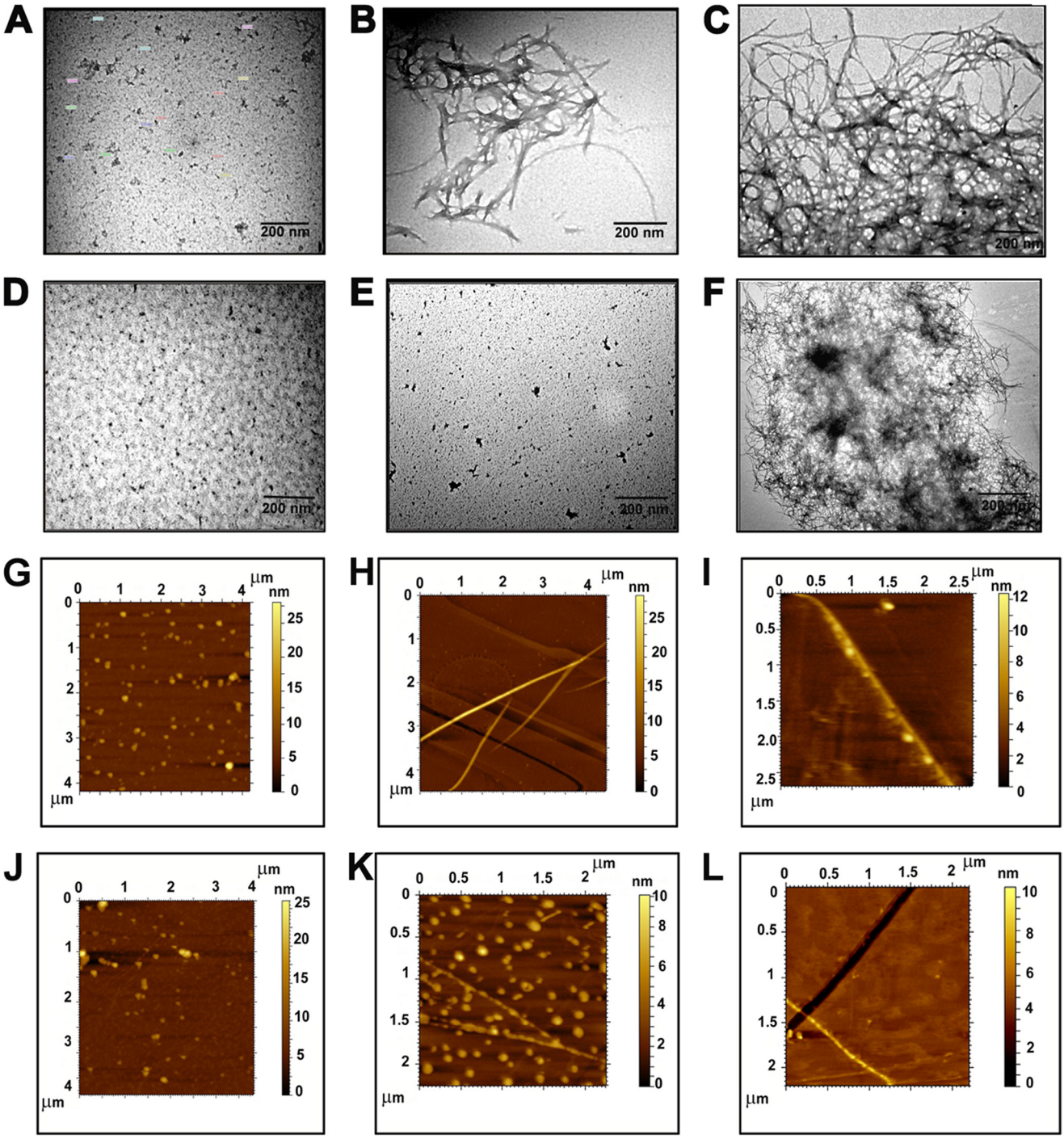

FIGURE 5. **Change of morphology of Aβ40/42 fibril as observed from TEM (*A–F*) and topographic AFM images (*G–L*).** *A*, Aβ42 monomer (5 μM). *B* and *C*, Aβ40 (5 μM) and Aβ42 (5 μM) fibrillar form obtained after incubation of respective monomers for 7 days at 37 °C. *D–F*, preformed Aβ42 fibril (5 μM) after incubation for 24 h in the presence of RVV-V (1 μM), R_{mix} (1 μM), and NS_1, respectively. The *bar* represents magnification that is uniformly maintained. Similar results were obtained with Aβ40 fibrils (data not shown). *G*, Aβ42 monomer (5 μM) showing diameter of 35–45 nm. *H* and *I*, rod-like image of fibrils detected after 7 days of aging of Aβ40 and Aβ42 monomers, respectively. *J* and *K*, preformed Aβ42 fibril after 24 h of incubation at 37 °C with R_{mix}. In *K*, spherical monomer, oligomer, and disrupted protofibrils are visible. *L*, fibrillar morphology of Aβ42 retained after incubation with NS_1 under identical conditions.

well as protection of human neuronal cells from Aβ-induced cytotoxicity. RVV-V is a glycoprotein possessing one glycosylation site near the C terminus (27). Absence of the specific residues (Arg^{1545}-Ser^{1546}) in the Aβ peptide discards the possibility of proteolytic cleavage of the Aβ peptide by RVV-V. This assumption is supported by the MALDI-TOF analysis, which showed that RVV-V produces only monomeric form of Aβ peptide when incubated with its higher oligomers and failed to generate peptides lower than 4 kDa. Therefore, disassembly of the preformed fibril by proteolysis is not possible; on the other hand, RVV-V digested by proteolytic enzymes showed inhibition of fibrillization (Fig. 1*F*). This raises the possibility of disrupting the fibril by β-sheet breaker peptides so generated, which might be intercalating and inhibiting the Aβ fibrillogen-

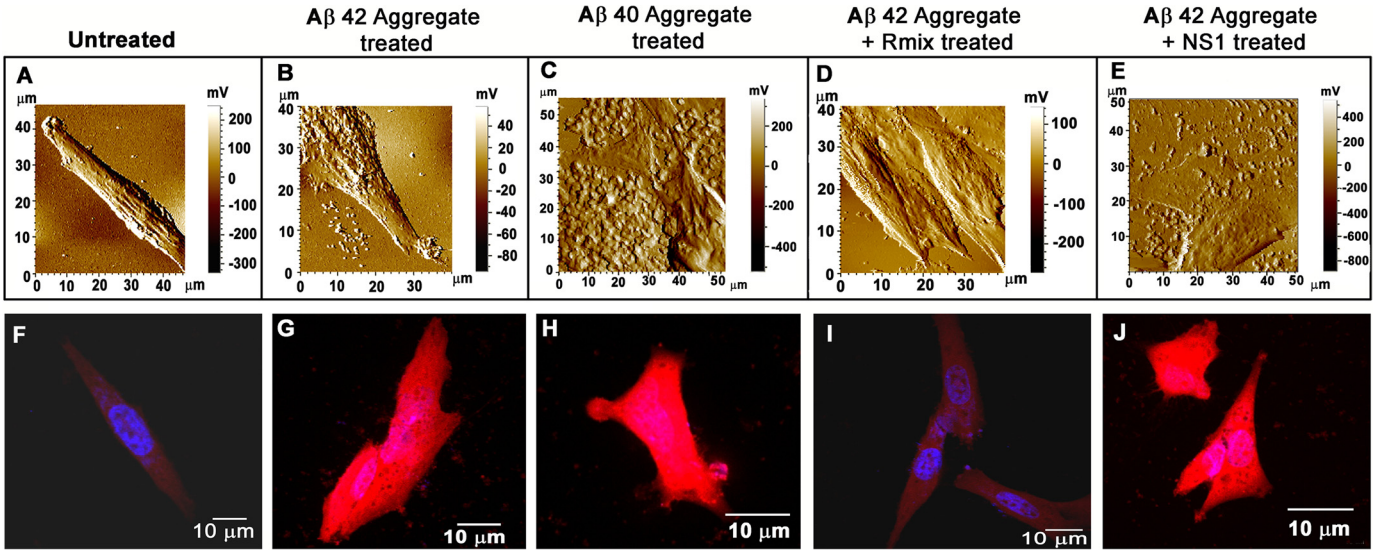

FIGURE 6. **Inhibition of Aβ40/42-induced cytotoxicity of SH-SY5Y cells by peptides as observed from AFM (*A–E*) and confocal (*F–J*) images.** *A*, untreated cell. *B* and *C*, formation of Aβ40 and Aβ42 (10 μM) aggregates on cell surface after incubation with preformed fibrils for 48 h at 37 °C. *D*, absence of the aggregates on the cell surface after incubation of the cells with Aβ42 fibril preincubated with R_{mix}. *E*, deposits of Aβ42 aggregates pretreated with NS_1 on cell surface. The mean height is obtained by taking multiple cursor measurements of the thickness of the fibrils through several representative images. The distribution of heights is presented as a histogram for each AFM view. In confocal images, the *bright red color* (secondary antibody conjugated with Alexa Fluor 633) and *blue color* (DAPI) indicate the presence of Aβ40/42 peptide-oligomer and nucleus of the cells, respectively. *F*, untreated cells showing very faint expression of Aβ42. *G*, cells treated with Aβ40 soluble oligomer (10 μM) showing intense *red color*, indicating localization of Aβ40 inside the cells. In this image, the cells have markedly different morphology from untreated cells. Localization of Aβ40 within the nucleus is clearly revealed from the image. *H*, cells treated with Aβ42 soluble oligomer (10 μM) followed by Alexa Fluor 633 as stated earlier. *I*, cells treated with Aβ42 oligomer preincubated with R_{mix} showing morphology and expression of Aβ42 similar to those of untreated cells as shown in *F*. *J*, cells treated with Aβ42 oligomer pretreated with NS_1 showing failure of prevention of internalization of the Aβ42 oligomer. These images are representative profiles from at least three sets of independent experiments.

esis leading to restoration of its monomeric and oligomeric forms. To check this, synthetic peptides were designed using RVV-V as template. It was based on the knowledge obtained from *in vitro* studies and bioinformatics. The small peptides which might have hydrophobic interaction with the QKLVFFA region of Aβ peptide might be intercalating into the β-sheet-rich region of Aβ aggregate, inhibiting further elongation of fibrils into the amyloid plaque and shifting the equilibrium toward the monomeric or small oligomeric form. This has been demonstrated by fibrillogenesis assay and microscopic analysis. Recently, computational and experimental data have elucidated the mechanism of fibril growth which proceeds via two steps. The initial step is nucleation which is driven by nonspecific hydrophobic interactions followed by a conformational conversion to ordered β-sheet structures by the formation of interchain hydrogen bonds (28–30). Thus, a viable strategy to design therapeutic molecules is to screen for compounds that can bind to preformed fibrils, shifting the equilibrium toward prefibrillar states. It has been shown that peptides that incorporate proline (β-sheet breaker) and *N*-methylated amino acids have the ability to disassemble mature Aβ fibrils (31–33). There are other reports on antiaggregation molecules like synthetic peptides, small dye molecules, polyphenols, and lipids (34).

In this context, we speculated how the peptides interact with Aβ aggregate leading to its near complete dissociation (Scheme 1). In this process, it is obligatory that the peptides interact with the aggregate to form [$Aβ_{agg}$-peptide] adduct. Because the dissociation reaction proceeds to near completion, it is indicative that this adduct is short lived. The natural course of degradation of this adduct may proceed through two pathways: it may be reduced to an [$Aβ_{oligo}$-peptide] complex which in due course

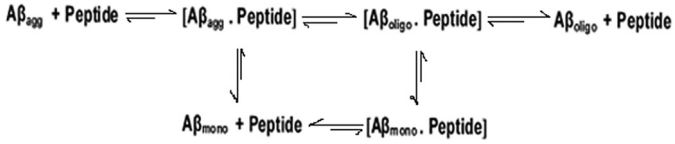

SCHEME 1. **Proposed interactions between different forms of Aβ and synthetic peptides.**

may be dissociated to $Aβ_{oligo}$ and the peptide; alternately, the adduct may be directly reduced to $Aβ_{mono}$ and the peptides. The alternate pathway may, of course, involve stepwise dissociation of the monomer. It also needs to be addressed at the end whether the peptide remains free or bound to small oligomers or monomers. This has implications for understanding the equilibrium between Aβ species and the peptides that inhibit the growth of aggregate and how Aβ is taken up into the cells in presence of the peptides. Mass spectrometric results of Fig. 3 are supportive of the fact that the adduct [$Aβ_{oligo}$-peptide] is almost exclusively dissociated from Aβ monomer and free peptides. Existence of the Aβ dimer was barely detectable whereas higher mers were absent. Free peptides but no [Aβ-peptide] adduct was detected. It was ensured that the MALDI analysis was done at the lowest energy of laser beam. Under that condition, protein-peptide complexes are not dissociated. Insignificant toxicity imparted to cells by the dissociated Aβ aggregate is indirect evidence of the absence of oligomers that are otherwise toxic. Thus it appears that the Aβ in its monomeric or at most dimeric form bind to the peptides whereas the equilibrium heavily favors their dissociated states preventing reformation of the oligomer *en route* aggregation.

Despite these encouraging findings, the biggest hurdle continuing until today is to deliver drugs into the brain to treat the

neurological disorders/diseases as most of these targets are intractable for drug development. The major limitation of the peptides as potential drug is their rapid degradation in biological fluids and tissues, immunogenicity, and poor bioavailability. For the treatment of neurological disorders, a drug must be able to penetrate the tight and selective blood-brain barrier (BBB), which supports the brain with high nutrient and allows the flow of small hydrophobic molecules, restricting the uptake of any microscopic objects and large or hydrophilic molecules (35). For a peptide, several factors such as size, molecular mass, flexibility, conformation, properties of constituent amino acids, and their sequence affect its ability to cross the BBB (36). Molecules having rotatable bonds and greater than 450 Da are restricted by the BBB (37). The BBB becomes more permeable during inflammation and allows some antibiotics and phagocytes to move across (38). This information is useful for drug delivery.

The cytotoxicity assay showed near complete viability of cell after treatment of preformed fibril by RVV-V-derived small peptides. Among these peptides, R_4 showed best consistency in preventing Aβ oligomer induced cytotoxicity in all the assays. It is also evident from confocal images that the peptides bind to the Aβ fibril and inhibit its internalization within the cell, but the exact mechanism remains to be elucidated. R_4 is of 595 Da which stands at the threshold value for BBB permeability. For the smaller peptides, the inhibitory potential is quite low compared with R_4. Another important observation is the ineffectiveness of nonspecific peptides for inhibition of fibrillization. Therefore, the importance of amino acid sequence and physical characters of the peptide in inhibiting fibrillogenesis is evident. The mixture composed of peptides of 300–800 Da also showed significant inhibition. These are probably peptides of variable lengths incorporated at different sites of the fibril affecting its conformation and stability. It is noteworthy that in neuroinflammation, disruption of BBB occurs, which allows quite large molecule to pass through it (35). Therefore, our approach of designing a peptide inhibitor from a natural source has rational grounds. At present, there is no effective treatment for AD. *In vivo* efficacy of many of the antiaggregation molecules has been validated in amyloid animal models, but extrapolation of these findings to the human condition is often found to be unreliable and unsafe (39). Despite these drawbacks, the endeavor toward the production of selective, more effective, and safer medicines to treat the diseases are moving forward. The duel potency of venom protein-derived peptides for inhibition of amyloidosis as observed from cell viability against toxicity and destabilization of amyloid to monomeric entities offers a good opportunity to explore these molecules as a therapeutic agent for both prevention and maintenance of the status quo in AD.

Acknowledgments—We thank T. Muruganandan, Dr. Aparna Laskar, Diptadeep Sarkar, and Dr. Ramdhan Majhi for AFM, TEM, confocal imaging, and amino acid sequencing respectively. We thank Prof. Subrata Pal, Department of Life Sciences and Biotechnology, Jadavpur University, Kolkata, for providing cell culture facility. The neuroblastoma cell line was generously given by Drs. K. P. Mohanakumar and Sumantra Das of this institute.

REFERENCES

1. Bitan, G., Kirkitadze, M. D., Lomakin, A., Vollers, S. S., Benedek, G. B., and Teplow, D. B. (2003) Amyloid β-protein (Aβ) assembly: Aβ40 and Aβ42 oligomerize through distinct pathways. *Proc. Natl. Acad. Sci. U.S.A.* **100,** 330–335
2. Friedrich, R. P., Tepper, K., Rönicke, R., Soom, M., Westermann, M., Reymann, K., Kaether, C., and Fändrich, M. (2010) Mechanism of amyloid plaque formation suggests an intracellular basis of Aβ pathogenicity. *Proc. Natl. Acad. Sci. U.S.A.* **107,** 1942–1947
3. Finder, V. H., and Glockshuber, R. (2007) Amyloid-β aggregation. *Neurodegener. Dis.* **4,** 13–27
4. Sakono, M., and Zako, T. (2010) Amyloid oligomers: formation and toxicity of Aβ oligomers. *FEBS J.* **277,** 1348–1358
5. Huang, T. H., Yang, D. S., Plaskos, N. P., Go, S., Yip, C. M., Fraser, P. E., and Chakrabartty, A. (2000) Structural studies of soluble oligomers of the Alzheimer β-amyloid peptide. *J. Mol. Biol.* **297,** 73–87
6. De Felice, F. G., Houzel, J. C., Garcia-Abreu, J., Louzada, P. R., Jr., Afonso, R. C., Meirelles, M. N., Lent, R., Neto, V. M., and Ferreira, S. T. (2001) Inhibition of Alzheimer's disease β-amyloid aggregation, neurotoxicity, and *in vivo* deposition by nitrophenols: implications for Alzheimer's therapy. *FASEB J.* **15,** 1297–1299
7. Pearson, H. A., and Peers, C. (2006) Physiological roles for amyloid β peptides. *J. Physiol.* **575,** 5–10
8. Abramov, E., Dolev, I., Fogel, H., Ciccotosto, G. D., Ruff, E., and Slutsky, I. (2009) Amyloid-β as a positive endogenous regulator of release probability at hippocampal synapses. *Nat. Neurosci.* **12,** 1567–1576
9. Deane, R., Bell, R. D., Sagare, A., and Zlokovic, B. V. (2009) Clearance of amyloid-β peptide across the blood-brain barrier: implication for therapies in Alzheimer's disease. *CNS Neurol. Disord. Drug Targets* **8,** 16–30
10. Benilova, I., Karran, E., and De Strooper, B. (2012) The toxic Aβ oligomer and Alzheimer's disease: an emperor in need of clothes. *Nat. Neurosci.* **15,** 349–357
11. Gestwicki, J. E., Crabtree, G. R., and Graef, I. A. (2004) Harnessing chaperones to generate small-molecule inhibitors of amyloid β aggregation. *Science* **306,** 865–869
12. Feng, Y., Wang, X. P., Yang, S. G., Wang, Y. J., Zhang, X., Du, X. T., Sun, X. X., Zhao, M., Huang, L., and Liu, R. T. (2009) Resveratrol inhibits β-amyloid oligomeric cytotoxicity but does not prevent oligomer formation. *Neurotoxicology* **30,** 986–995
13. Koren, J., 3rd, Jinwal, U. K., Lee, D. C., Jones, J. R., Shults, C. L., Johnson, A. G., Anderson, L. J., and Dickey, C. A. (2009) Chaperone signaling complexes in Alzheimer's disease. *J. Cell. Mol. Med.* **13,** 619–630
14. Westermann, J. C., and Craik, D. J. (2008) NMR in peptide drug development, *Methods Mol. Biol.* **494,** 87–113
15. Drag, M., and Salvesen, G. S. (2010) Emerging principles in protease-based drug discovery. *Nat. Rev. Drug Discov.* **9,** 690–701
16. Li, J. W., and Vederas, J. C. (2009) Drug discovery and natural products: end of an era or an endless frontier. *Science* **325,** 161–165
17. Shaw, C. (2009) Advancing drug discovery with reptile and amphibian venom peptides: venom-based medicines. *Biochem. Soc.* **31,** 34–37
18. Tsai, I. H., Lu, P. J., and Su, J. C. (1996) Two types of Russell's viper revealed by variation in phospholipases A_2 from venom of the subspecies. *Toxicon* **34,** 99–109
19. Kisiel, W., and Canfield, W. M. (1981) Snake venom proteases that activate blood coagulation factor V. *Methods Enzymol.* **80,** 275–285
20. Marsh, N. A. (1998) Use of snake venom fractions in the coagulation laboratory. *Blood Coagul. Fibrinolysis* **9,** 395–404
21. Shevchenko, A., Tomas, H., Havlis, J., Olsen, J. V., and Mann, M. (2006) In-gel digestion for mass spectrometric characterization of proteins and proteomes. *Nat. Protoc.* **1,** 2856–2860
22. LeVine, H., 3rd (1993) Thioflavin T interaction with synthetic Alzheimer's disease β-amyloid peptides: detection of amyloid aggregation in solution. *Protein Sci.* **2,** 404–410
23. Kuznetsova, I. M., Sulatskaya, A. I., Uversky, V. N., and Turoverov, K. K. (2012) Analyzing thioflavin T binding to amyloid fibrils by an equilibrium microdialysis-based technique. *PLoS One* **7,** e30724
24. Adessi, C., Frossard, M. J., Boissard, C., Fraga, S., Bieler, S., Ruckle, T.,

Vilbois, F., Robinson, S. M., Mutter, M., Banks, W. A., and Soto, C. (2003) Pharmacological profiles of peptide drug candidates for the treatment of Alzheimer's disease. *J. Biol. Chem.* **278,** 13905–13911
25. Shearman, M. S., Hawtin, S. R., and Tailor, V. J. (1995) The intracellular component of cellular 3-(4,5 dimethylthiazol-2-yl)-2,5diphenyltetrazolium bromide (MTT) reduction is specifically inhibited by β-amyloid peptides. *J. Neurochem.* **65,** 218–227
26. Strober, W. (1997) *Current Protocols in Immunology*, pp. A. 3B. 1-A. 3B. 2, John Wiley & Sons, New York
27. Tokunaga, F., Nagasawa, K., Tamura, S., Miyata, T., Iwanaga, S., and Kisiel, W. (1988) The factor V-activating enzyme (RVV-V) from Russell's viper venom: identification of isoproteins RVV-V(α), -Vβ, and -Vγ and their complete amino acid sequences. *J. Biol. Chem.* **263,** 17471–17481
28. Ono, K., Condron, M. M., and Teplow, D. B. (2009) Structure-neurotoxicity relationships of amyloid β-protein oligomers. *Proc. Natl. Acad. Sci. U.S.A.* **106,** 14745–14750
29. Cheon, M., Chang, I., Mohanty, S., Luheshi, L. M., Dobson, C. M., Vendruscolo, M., and Favrin, G. (2007) Structural reorganisation and potential toxicity of oligomeric species formed during the assembly of amyloid fibrils. *PLoS Comput. Biol.* **3,** 1727–1738
30. Bellesia, G., and Shea, J. E. (2009) Diversity of kinetic pathways in amyloid fibril formation. *J. Chem. Phys.* **131,** 111102
31. Bett, C. K., Ngunjiri, J. N., Serem, W. K., Fontenot, K. R., Hammer, R. P., McCarley, R. L., and Garno, J. C. (2010) Structure-activity relationships in peptide modulators of β-amyloid protein aggregation: variation in α,α-disubstitution results in altered aggregate size and morphology. *ACS Chem. Neurosci.* **1,** 608–626
32. Soto, C., Sigurdsson, E. M., Morelli, L., Kumar, R. A., Castaño, E. M., and Frangione, B. (1998) β-Sheet breaker peptides inhibit fibrillogenesis in a rat brain model of amyloidosis: implications for Alzheimer's therapy. *Nat. Med.* **4,** 822–826
33. Gordon, D. J., Tappe, R., and Meredith, S. C. (2002) Design and characterization of a membrane permeable *N*-methyl amino acid-containing peptide that inhibits Aβ(1–40) fibrillogenesis. *J. Pept. Res.* **60,** 37–55
34. Hawaes, C. A., Ng, V., and McLaurim, J.-A. (2009) Small molecule inhibitors of Aβ-aggregation and neurotoxicity. *Drug Dev. Res.* **70,** 111–124
35. de Vries, H. E., Kuiper, J., de Boer, A. G., Van Berkel, T. J., and Breimer, D. D. (1997) The blood-brain barrier in neuroinflammatory diseases. *Pharmacol. Rev.* **49,** 143–155
36. Witt, K. A., and Davis, T. P. (2006) CNS drug delivery: opioid peptides and the blood-brain barrier. *AAPS J.* **8,** E76–88
37. Abbott, N. J., Patabendige, A. A., Dolman, D. E., Yusof, S. R., and Begley, D. J. (2010) Structure and function of the blood-brain barrier. *Neurobiol. Dis.* **37,** 13–25
38. Phares, T. W., Kean, R. B., Mikheeva, T., and Hooper, D. C. (2006) Regional differences in blood-brain barrier permeability changes and inflammation in the apathogenic clearance of virus from the central nervous system. *J. Immunol.* **176,** 7666–7675
39. Van Dam, D., and De Deyn, P. P. (2006) Drug discovery in dementia: the role of rodent models. *Nat. Rev. Drug Discov.* **5,** 956–970